UNIVERSITY OF MICHIGAN
Department of Mechanical Engineering
Cavitation and Multiphase Flow Laboratory

Report No. UMICH 014456-1-I

PRESSURE PROBE CALIBRATION

by

M.K. De
Scott A. Barber
F.G. Hammitt

Financial Support Provided by:

Office of Naval Research
Contract No. NOOl4-77-C067

July 1976

List of Figures

List of Tables

1.0 Abstract

The purpose of this research program is to develop the ability to predict the damage rate caused by collapsing bubbles in a cavitation field. As explained in previous reports,[1, e.g.] a technique is being developed to enable damage rate prediction by examining the cavitation pulse spectrum. Measured damage rates have been correlated with bubble collapse pulse count spectra for water and sodium.

An "absolute" probe calibration has been made so that the correlations between pulse count energy spectrum and MDPR* can be reproduced by any suitably equipped laboratory without the required use of probe and electronic components identical to those which we have used here. The report also provides information concerning the methods involved in the probe calibrations.

* Mean Depth of Penetration Rate = volume loss rate/exposed area.

2.0 Introduction

One purpose of the present project is to determine whether a definite correlation exists between cavitation damage and the accompanying cavitation noise manifested by individual bubble collapse pulses. If such a correlation is found, eventual cavitation damage rates could then be predicted a priori, by simply measuring the cavitation bubble collapse pulse spectra. The practicality of the proposed method of cavitation damage prediction is dependent upon the degree to which the method can be standardized between laboratories. In order to compare pulse count data collected from various probes, the probes must be calibrated to determine their relative sensitivities. The purpose of this report is to present the method and results of our sonic probe calibrations.

Our development of this damage predicting technique followed a two-step process:

1) Ultrasonic cavitation damage tests were performed over a range of temperatures and pressures, and cavitation bubble collapse spectra were collected by means of a specially developed sonic wave-guide probe and related equipment, (Fig. 1). This type of probe was required because the tests included high-temperature sodium (1). This data was processed into a numerical equivalent, termed "spectral area", i.e. area under curve of number of pulses vs. pulse energy (Ref. 1). Actual damage rates to test specimens are determined as usual by weight loss. A plot

which relates cavitation damage rate (MDPR) to cavitation bubble collapse spectra is a result of these vibratory tests.

2) Similar cavitation bubble collapse spectra are to be collected from a flowing venturi device. Hopefully, the plots which relate vibratory damage to vibratory cavitation collapse spectra will also apply to various flowing systems, such as our projected venturi tests.

The cavitation 'noise' was processed by using a high-pass filter and a discriminant pulse counter. The counter was adjusted to count only pulses above certain set intensity values. During the course of the test, this setting then becomes the independent variable. The result, in graphical form, is a pulse spectrum curve of pulse intensity vs. number of counts. The area under the curve is the aforementioned spectral area.*

Figure 1 shows the electronic instrumentation. The horn was driven at 20 kHZ by the Branson power supply at horn amplitude of 1.5 mils. The pulse from the wave guide probe crystal was initially passed through a Kistler Model 566 charge amplifier set at 10 mv/pcb. The pulse was then amplified (20 db) in a Krohn-Hite Model 3322 filter-amplifier. The high-pass filter settings used in the above instrument were set at various frequency limits starting at 40 kHZ to filter out signals from the ultrasonic horn (20 kHZ) and other machine noise. The pulse count rate was made on a Baird Atomic Glow Tube Counter Model 1283.

In spite of the relatively crude pulse measuring set-up

* Figures 5-9 are typical curves of this type actually measured.

employed in these initial experiments in a vibratory cavitation damage facility, meaningful ($\lesssim$ 25% standard error) correlations have been obtained between pulse-count integrated energy spectrum and measured damage rate (MDPR), (Ref. 1).

For water, a simple linear relationship between spectral area and measured MDPR was obtained over a considerable temperature and pressure range, of the type (Ref. 1).

$$MDPR = C_1 \text{ (Area)} - C_2 \quad \text{- - - - - - - - - - - - (1)}$$

where "Area" is the area under the pulse-count spectrum curve,

$$\text{i.e., Area} = \int_0^\infty N \text{ (Pht)} \; d \text{ (Pht)} \quad \text{- - - - - (2)}$$

and Pht is "pulse height selector setting" on the Baird Atomic Glow Tube Counter. The pulse height is proportional to the pressure pulse produced by the collapsing bubble, which is related to the energy produced by the bubble collapse.

3. Probe Calibration

The work here reported essentially describes our probe calibration in a non-cavitating bench rig, involving a hammer-pendulum (Fig. 2). This then provides a means for comparing the sensitivities of the different probes used both here and at Westinghouse Advanced Reactor Division (W-ARD), see ref. 1.

In principle, cavitation collapse pulses are to be detected by a pressure transducer, i.e.,"probe." Two types are involved. For one the active element is immersed in the test liquid such as the Kistler probe. The other is a "wave-guide" probe (Fig. 3) with the active element not immersed in the liquid. The reason for using a "wave-guide" probe in sodium for our experiments was that a microprobe with suitable high temperature crystal was not available at that time. We have since developed such a probe with high temperature crystal which can operate in sodium to 500^{o}F (Fig. 4).

Pressure applied to the face of the transducer is converted to a force acting on the transducer ceramic, which then generates an electrical charge output proportional to the pressure input. The basic sensitivity of these instruments is in terms of unit charge per unit pressure, and is normally expressed as pico-coulombs per psi (pCb/psi). The charge amplifier is a DC voltage amplifier with a capacitive feedback path from the low-impedance output circuit to the high impedance input circuit. The output voltage which results from a charge signal input is returned to the input circuit through the feedback capacitator, in the direction to maintain the input circuit voltage at or near zero. The net charge from the input circuit is stored in the feedback capacitator, producing a potential difference across it equal to the value of charge divided by the value of capacitance, and this potential difference determines the relationship of the output voltage signal to the input charge signal. The transfer characteristic, or "gain," of the amplifier is dependent only on the value of the feedback capacitator, and is unaffected by time, temperature, or line voltage variations.

The details of the acoustic wave delivered to the crystals in the two types of probes may differ. However, pressure pulses resulting from collapsing bubbles are measured in either case. Other uncertainties involve the precise form of bubble collapse. For example, the bubbles from which the signal originates could be collapsing at different distances from the probe, or adjacent to the

probe tip, perhaps producing liquid microjet impingement.

3.1 Calibration Procedure - General

As previously mentioned, probe calibration provides a means by which cavitation noise data collected from different sonic probes can be compared. This calibration requires at least a very approximate simulation of bubbles collapsing in a cavitating field. For our calibration, a hammer-pendulum system was used, where the energy imparted to the probe can be easily determined. Figure 2 shows the calibration apparatus.

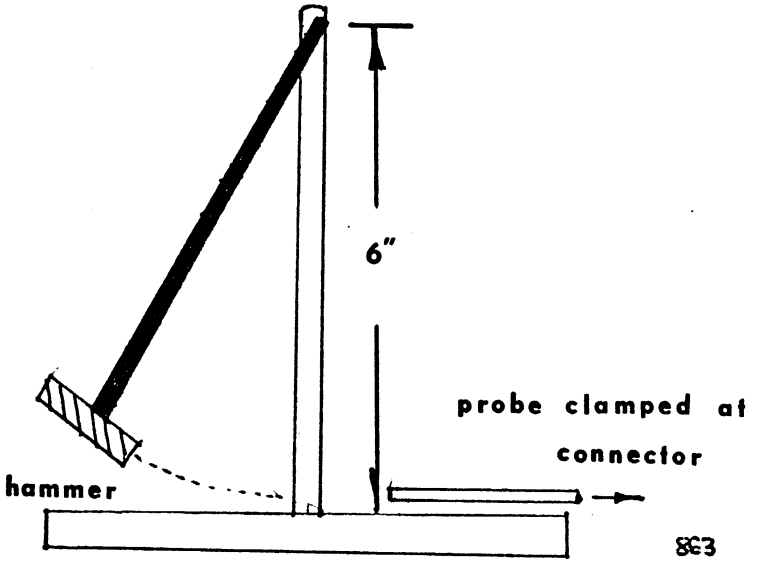

FIG 2.

The hammer can be released from different angles in order to impart measurable quantities of energy to the end of the probe being calibrated.

Two types of probes were calibrated: 1) two "wave-guide" probes, one used in our vibratory sodium cavitation tests and the other in the W-ARD venturi sodium tests (Fig. 3); 2) two direct submergence probes (Kistler Model 603-A with quartz crystal) and U-M probe (Fig. 4).

The wave-guide probes have PZT crystals which are attached to the end of a stainless steel rod (Fig. 3). The acoustic pulse is transmitted through the steel rod to the crystal. In the case of the direct submergence probes, the crystal is enclosed and sealed at the tip of the probe so that there is less transmission loss and alteration of the wave.

Due to the different constructions of the two types of probes, two different methods of probe calibration were used. For the wave-guide probe, we used an

electronic "chain" identical to the apparatus used for our earlier water and sodium tests to assure the maximum applicability of the calibration. For the direct submergence probes, we used an oscilloscope to record the response of the probe, since "pulse-counting" was not practical for this type of probe with the single-blow hammer impact. (Fig. 1)

3.2 Wave Guide Probes

The acoustic probe was impacted by the pendulum hammer from a specific angle, θ. Since there is very little rebound, the energy imparted to the probe can be calculated as being the potential energy at the initial position for such a pendulum (Fig. 2).

Potential Energy = $mgl(1 - \cos\theta)$, where l is length of arm.

As in our actual cavitation experiments, a pulse spectrum curve is obtained for each wave-guide probe. By varying the pulse height selector of the counter, we arrive at a pulse height spectrum curve for the probe for a particular filter frequency setting. A diagram of the electronic chain is shown in Fig. 1. The area under the curve is assumed to be proportional to the energy imparted to the probe. Thus, this area is indicative of the sensitivity of the probe.

Figures 5-9 are the spectral area curves for the two wave-guide probes calibrated. As already mentioned, one probe was used at Westinghouse for their liquid sodium venturi experiments (W-ARD) and the other at our laboratory (U-M) for our vibratory tests. These probes, nominally identical, were both fabricated by U-M. Table 1 is a summary of the data.

Frequency Setting	U-M	W-ARD	$\frac{\text{U-M}}{\text{W-ARD}}$
60 kHz	19.1	12.2	1.57
70 kHz	20.0	8.45	2.37
80 kHz	13.5	7.58	1.78
90 kHz		5.73	

Table 1

Comparative Areas For Wave-Guide Probes

Average $\frac{\text{U-M}}{\text{W-ARD}} = 1.9$

From the data presented in the table* we can assume that the U-M probe was ~ 1.9 more sensitive to pressure fluctuations than the W-ARD probe. Therefore, spectral areas formed from data collected by the two probes should have the following relationship:

$$\text{Area}_{\text{U-M}} = 1.9 \times \text{Area}_{\text{W-ARD}}$$

This relationship should hold true if all other variables, such as equipment and equipment settings, are held constant.

3.3 Direct Submergence Probes

Due to their construction, the direct submergence probes were calibrated in a fashion different from the wave-guide probes. As in the wave-guide probes, the hammer-pendulum apparatus was used to impart measurable impulses.

The direct submergence probes were calibrated by impacting the tip of the probe with various measurable impulses determined by simple calculations from the hammer parameters. The output of the probe was then measured using an oscilloscope. The probe was struck by the hammer, which was released at various angles. The resulting pulse from the probe was passed through a charge amplifier at 10 mv/pcb and a frequency filter with a 20 db gain, and then the output was displayed on an oscilloscope. Pictures were taken of the output, and values of output intensity and duration were determined from the displays. Figure 10 shows typical oscilloscopes obtained.

* Numerical average neglecting 40 kHZ which previous experience has shown to be too close to horn drive frequency of 20 kHZ for meaningful results.

3.3.1 Theory

In this case a pressure pulse of known amplitude was imparted to the tip of the probe. The pressure pulse amplitude was not calculated for the wave-guide probes because of the attenuation and alteration of the pulse through the stainless steel rod before reaching the crystal. This complicates matters and thus energy concepts were used.

The direct submergence probes were hit by the pendulum hammer (Fig. 2) from different angles, thus imparting different amounts of energy. Under these conditions the force on the gage during an impact is $F = CV/kd$ or $P = CV/kdA$ where C is the capacitance of the electronic chain shown in Fig. 1, V is the voltage output on the scope, k is the gage constant, and d the piezoelectric constant. Now,

$$\int F dt = \int m \frac{dV}{dt} \cdot dt = m \int dV = m \left[V_f - V_i\right]$$

Since the initial velocity V_i of the pendulum is zero, Impulse = $m V_f$. Potential Energy of the pendulum at initial position is equal to the kinetic energy at the final position. Therefore, $V = \left[2 g h_i\right]^{1/2}$ where h_i is initial pendulum elevation above final position h_o. Therefore, $m \left[2 g h_i\right]^{1/2} = \int F dt = 2/3 F_{max} \tilde{\tau}$ where $\tilde{\tau}$ is the duration of impact and $F_{average} = 2/3 F_{max}$, according to previous studies (3). Therefore, $m \left[2g(h)_i\right]^{1/2} = \frac{C}{kd} \cdot \frac{2V_{max} \tilde{\tau}}{3}$.

3.3.2 Reduction of Experimental Calibration Data

$m\left[2g(h)\right]^{1/2}$ was plotted versus $V_{max}\tau$. A gain of 20 db* was used so $V_{max}/V_{in} = 10$ and, therefore, V_{max} was scaled down by a factor of 10, db = 20 log (V_{out}/V_{in}). The slope measured from the graph is $\frac{7 \times 10^{-2}}{1100 \times 10^{-7}} = 636.4$ The height $h = \ell(1-\cos\theta)$ is tabulated for different angles. $\ell = 3.91$ in $= 9.7 \times 10^{-2}$ m. m = .144 kgs.

The measured capacitance of the electronic chain was 2.4 nano Farads.

Kistler Probe

From the equation $m(2gh)^{1/2} = 2/3\left(\frac{CV_m\tau}{kd}\right)$ the slope $= 2/3\left(\frac{C}{kd}\right) = 636.4$

Therefore, kd = 2.51×10^{-12} volts. Diameter of gage tip = 0.5 cm.

Area of gage tip = 1.96×10^{-5} m^2 Slope = 2.03×10^{16} $\frac{N}{m^2 Cb}$

Slope = 2.94 psi/pcb. Charge Sensitivity = 0.35 $\frac{pcb}{psi}$

U-M Direct Submergence Probe

Slope = $2/3\ \frac{C}{kd} = 2.69$ therefore kd = 5.95×10^{-10}

Diameter of probe tip = 0.25 in. Area of probe tip = $3.17 \times 10^{-5} m^2$

Slope = 5.3×10^{13} $\frac{N}{m^2 Cb}$ $= 7.69 \times 10^{-3}$ $\frac{psi}{pcb}$ Charge Sensitivity = 130 $\frac{pcb}{psi}$

Thus the charge sensitivity of the U-M probe is 350X that of the Kistler. The two constants that determine the charge sensitivity of a probe are the piezoelectric constant (d) and the gage constant (k). Pressure $\propto \frac{1}{kd}$ (Charge) and thus the larger the constant, the larger the charge sensitivity pcb/psi. The piezoelectric constant of the PZT crystal in the U-M direct submergence probe is larger than the quartz crystal in the Kistler probe, but certainly not by the ratio between the charge sensitivities. The duration of the pulse in the U-M probe is of the order

* This is a 'nominal' value, and may need to be examined more closely later.

of milli-seconds, compared to micro-seconds for the Kistler probe. The charge sensitivity for the U-M probe is much larger because of the large gage constant resulting from the long duration of the impact. Certain internal vibrations within the probe may be part of the cause for this. The design is being further investigated for later improvements.

3.4 Overall Comparisons and Calibration Results

Table 4 shows the overall comparison between the two direct-submergence and the two wave-guide probes in terms of "spectrum area" in units of counts x volts, delivered at the end of the electronic chain, as a function of frequency cut-off. It may be possible at a later date to provide more precise data of this type, and a direct comparison between the wave-guide and direct-submergence probes can also be provided by exposing them each to cavitation regimes in both vibratory horn and venturi. Hopefully, this can be accomplished in the relatively near future.

It will be noted that the output areas of all probes for a given momentum input are of the same order of magnitude, with that of the wave-guides being a factor of 2-3 more than that of the direct submergence. It seems reasonable that this is primarily due to the attenuation of the wave-guide, combined with possible resonance effects therein. That the Kistler and U-M direct submergence probes provide about the same output is apparently only fortuitous. Only a minimum frequency cut-off was used with the direct submergence probes, since the hammer pulse is otherwise severely attenuated.

4.0 Conclusions

The pressure pulses emitted by collapsing bubbles in a cavitation situation can be detected by sonic probes, both commercially available and specially designed. This cavitation "noise" can be processed and correllated with the resulting cavitation damage. It is evident at this time that cavitation damage in hydraulic machinery can be predicted by measuring the resulting cavitation bubble collapse spectra.

So that experimental data from various laboratories can be compared, calibration of the sonic probes is necessary. At the University of Michigan we have calibrated four (4) separate probes of two designs by using a hammer-pendulum apparatus to impart measurable and constant impulses to the probes.

Tables 3 and 4 show the final results of the probe calibrations. The "coefficients" relating spectral pulse count area to delivered momentum are of the order of magnitude for all probes.

In terms of pulse-charge sensitivity, the U-M direct submergence probe is $\sim$ 370 x more sensitive than the Kistler (Model 603-A). This is partially due to the greater sensitivity of the PZT ceramic as compared with the quartz crystal used in the Kistler, and mainly to the larger gage constant of the U-M probe.

5.0 References

1. F.G. Hammitt, etal., "Final Report - Argonne National Laboratory," ORA Report No. UMICH 013503-2-F, June 1976.

2. T.J. Costello, R.L. Miller, S.L. Schrock, "Cavitation Test," W-ARD, XARA-52045, May 1976, Westinghouse, Advanced Reactor Div.

3. M.C. Rochester, J.H. Brunton, "Influence of Physical Properties of Liquid on the Erosion of Solids," Erosion, Wear, and Interfaces with Corrosion, ASTM, STP 567, 1974, p. 128-151.

FIG. 1

BLOCK DIAGRAM OF ULTRASONIC VIBRATORY FACILITY

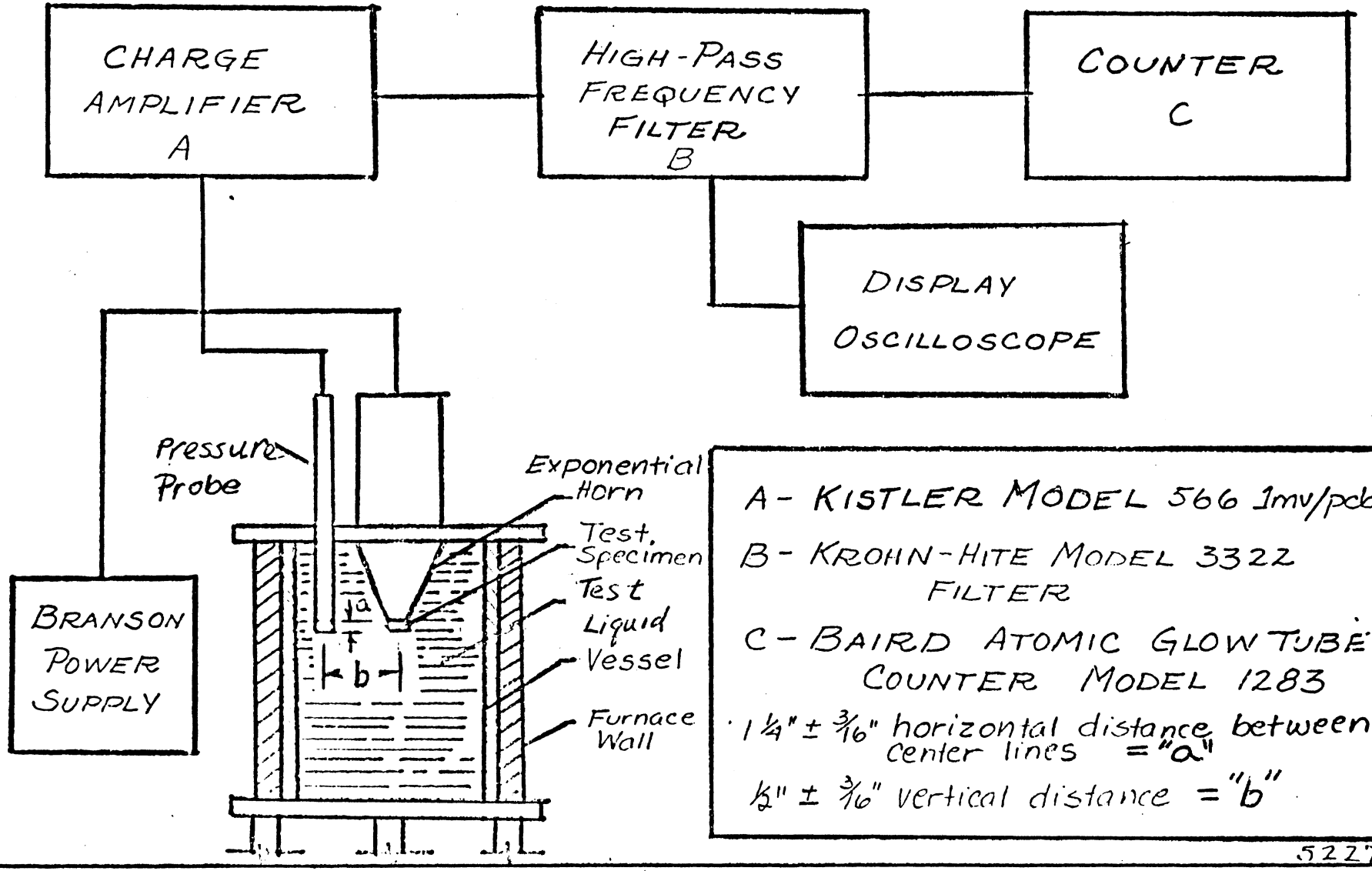

A - KISTLER MODEL 566 1mv/pcb

B - KROHN-HITE MODEL 3322 FILTER

C - BAIRD ATOMIC GLOW TUBE COUNTER MODEL 1283

1 1/4" ± 3/16" horizontal distance between center lines = "a"

1/2" ± 3/16" vertical distance = "b"

5227

J.A. FAUST 2-19-76

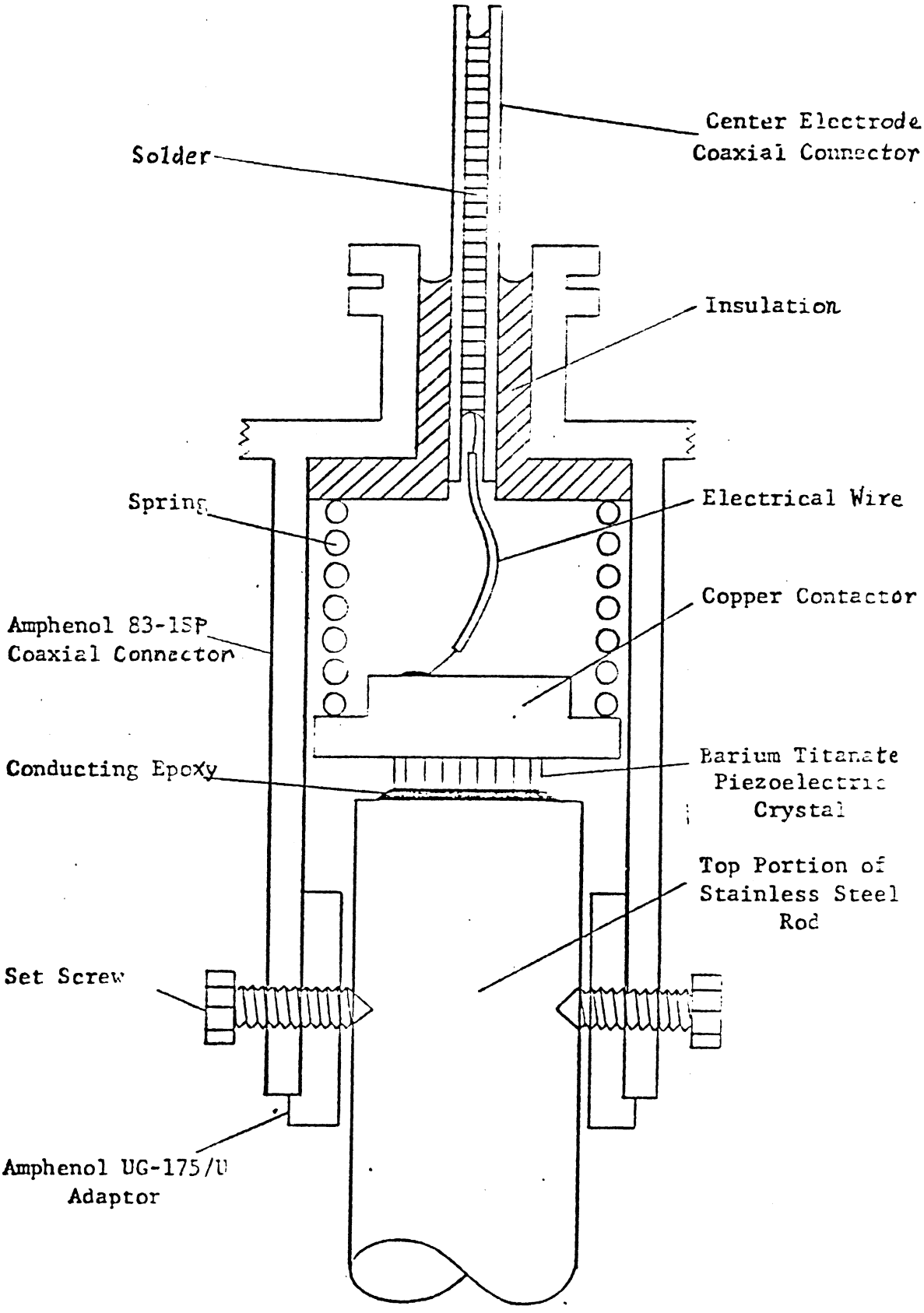
Center Electrode
Coaxial Connector
Solder
Insulation
Spring
Electrical Wire
Copper Contactor
Amphenol 83-1SP
Coaxial Connector
Conducting Epoxy
Barium Titanate
Piezoelectric
Crystal
Top Portion of
Stainless Steel
Rod
Set Screw
Amphenol UG-175/U
Adaptor
2639

FIG 3.

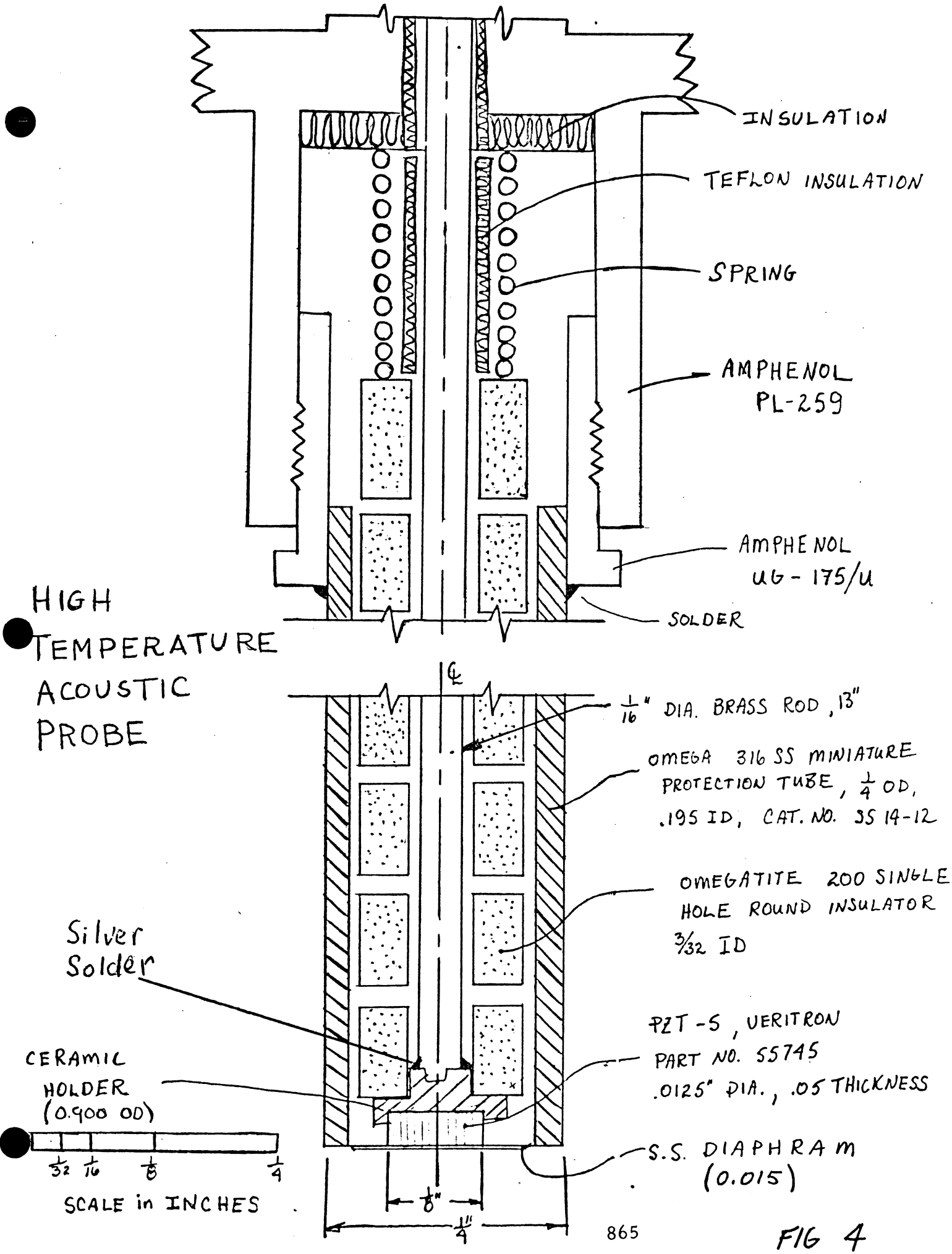
INSULATION
TEFLON INSULATION
SPRING
AMPHENOL PL-259
AMPHENOL UG-175/U
SOLDER
HIGH TEMPERATURE ACOUSTIC PROBE
℄
1/16" DIA. BRASS ROD, 13"
OMEGA 316 SS MINIATURE PROTECTION TUBE, 1/4 OD, .195 ID, CAT. NO. SS 14-12
OMEGATITE 200 SINGLE HOLE ROUND INSULATOR 3/32 ID
Silver Solder
PZT-5, VERITRON PART NO. 55745 .0125" DIA., .05 THICKNESS
CERAMIC HOLDER (0.900 OD)
S.S. DIAPHRAM (0.015)
1/32 1/16 1/8 1/4
SCALE in INCHES
1/8"
1/4"

FIG 4

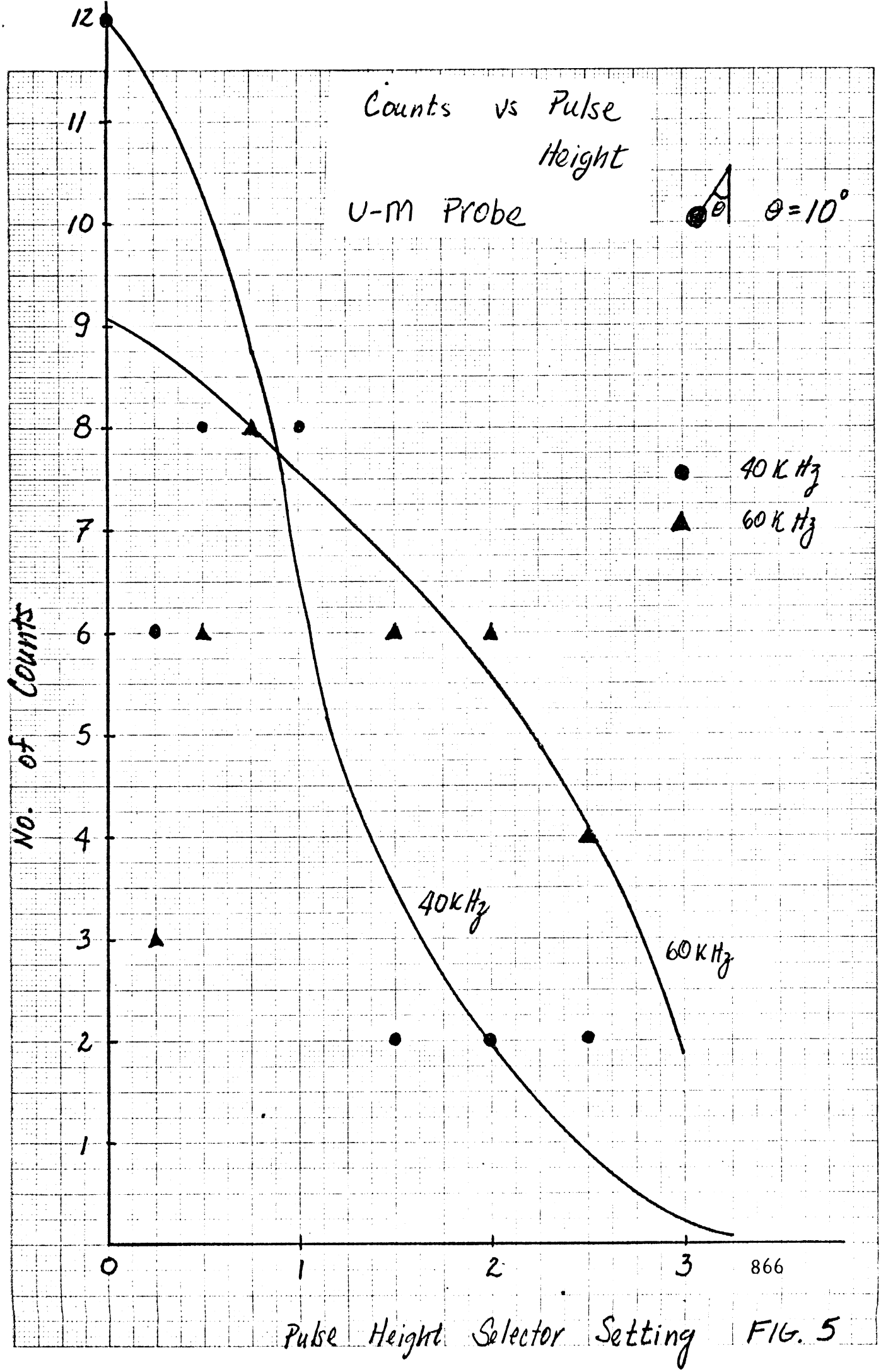

FIG. 5

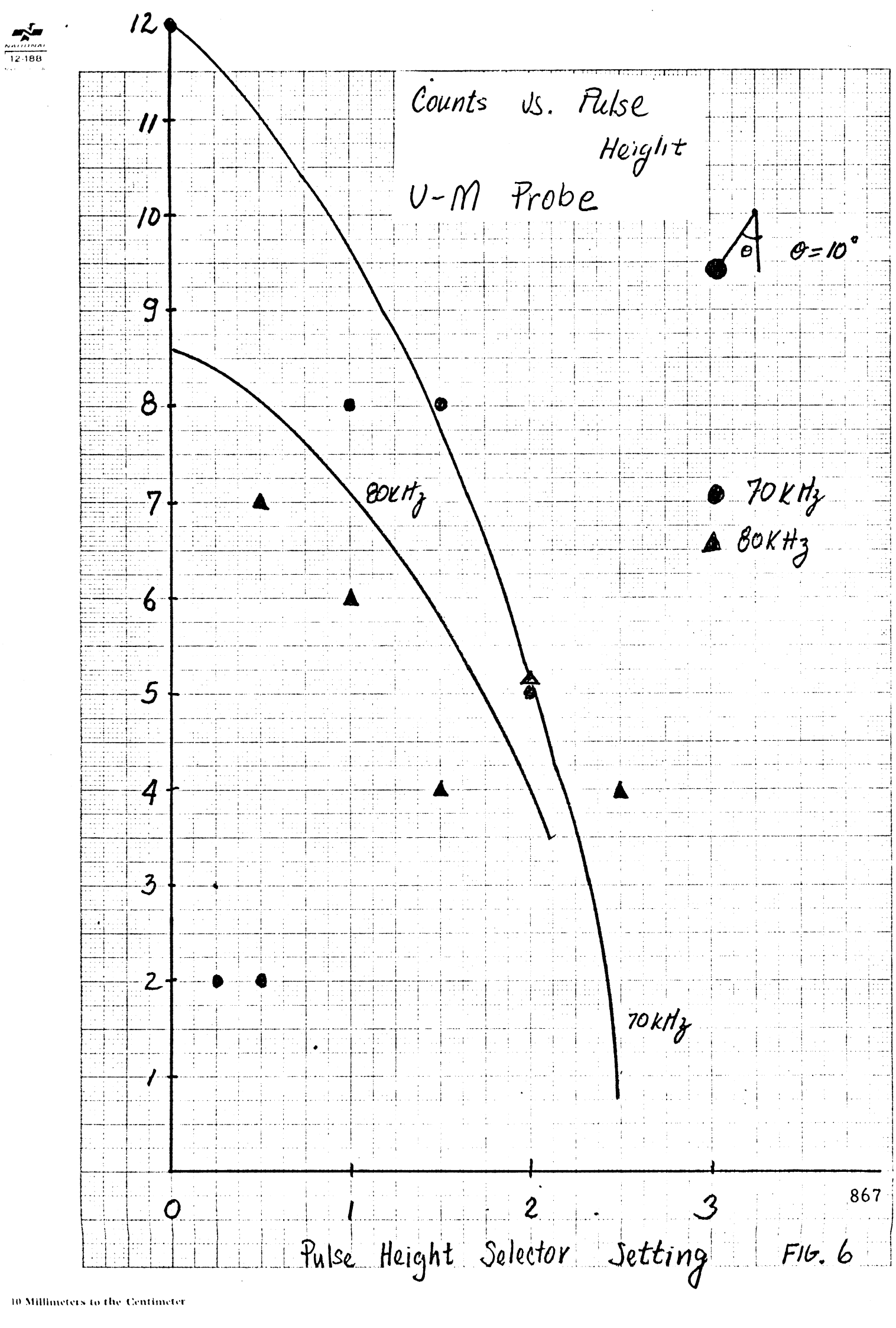

FIG. 6

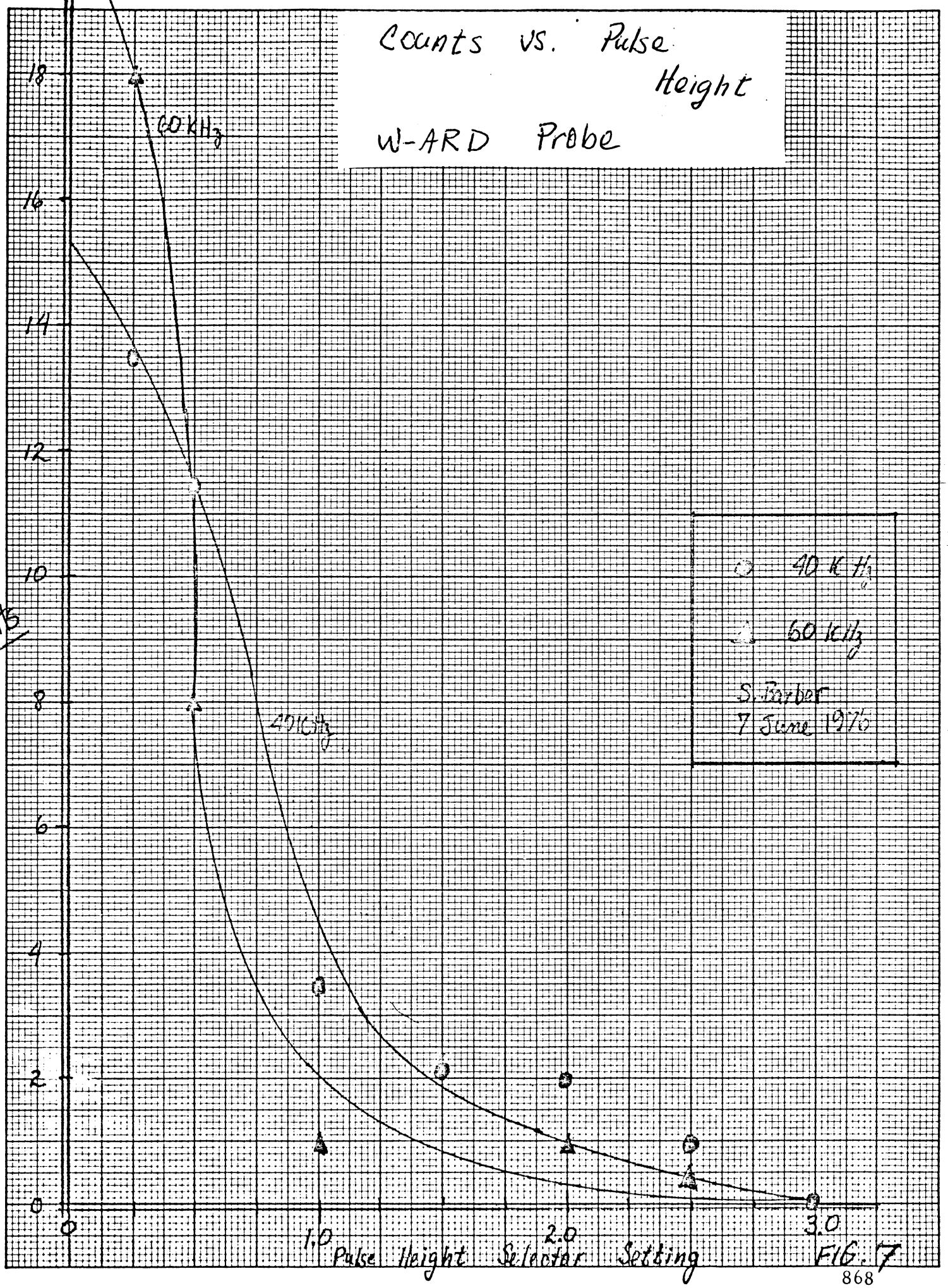

FIG. 7

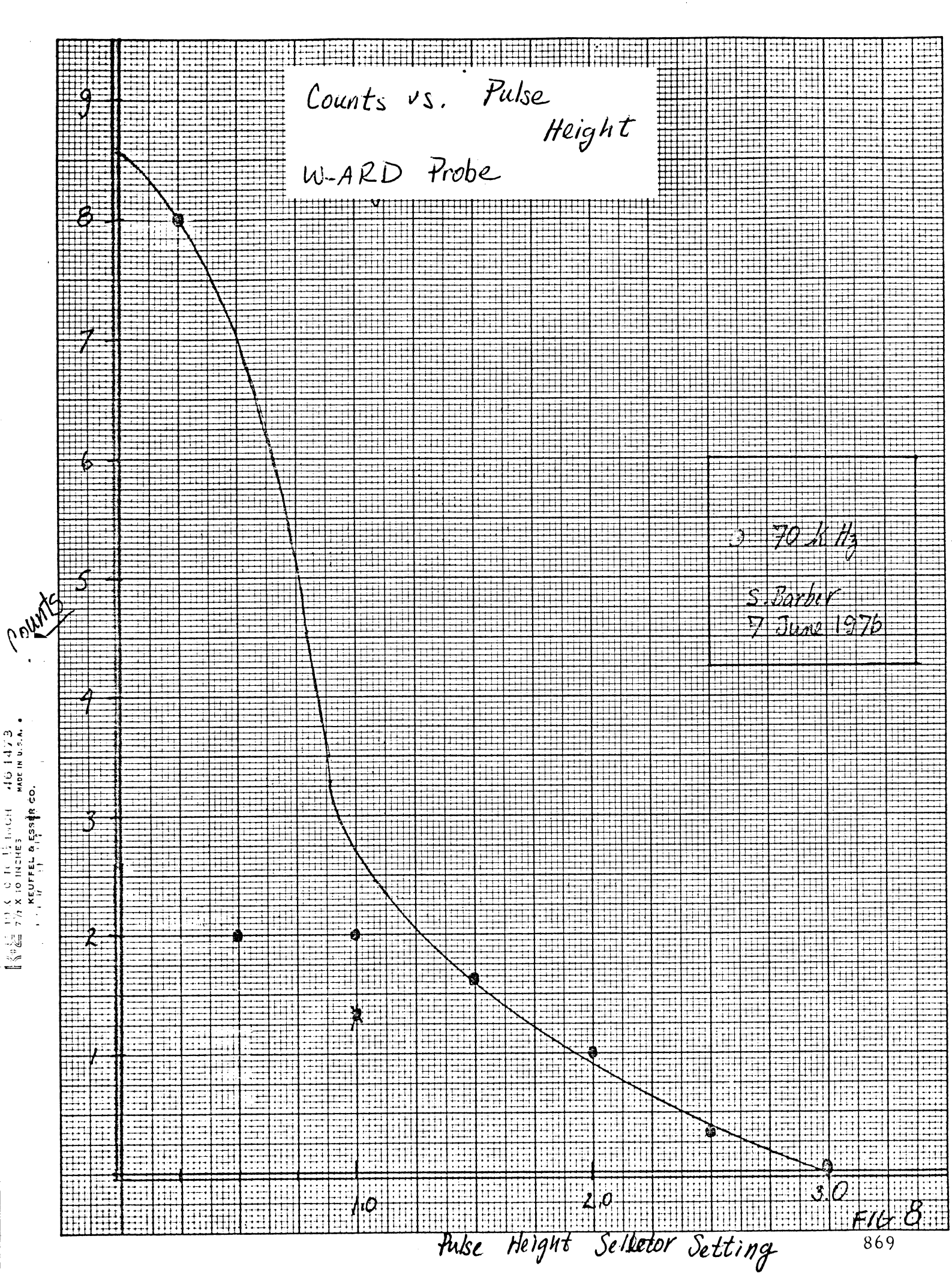
Counts vs. Pulse Height
W-ARD Probe
70 K Hz
S. Barber
7 June 1976
Counts
9
8
7
6
5
4
3
2
1
1.0
2.0
3.0
Pulse Height Selector Setting

FIG 8

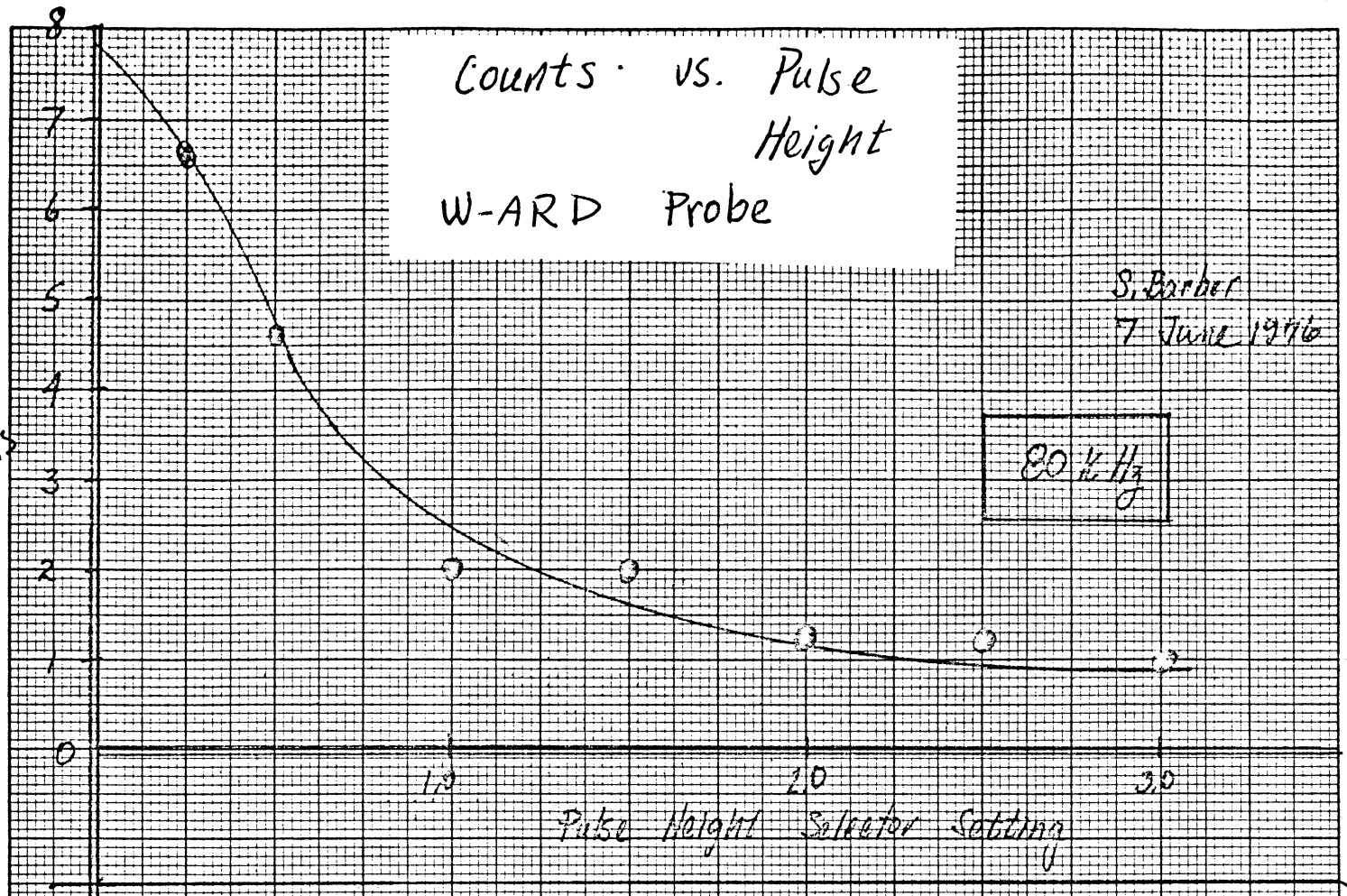

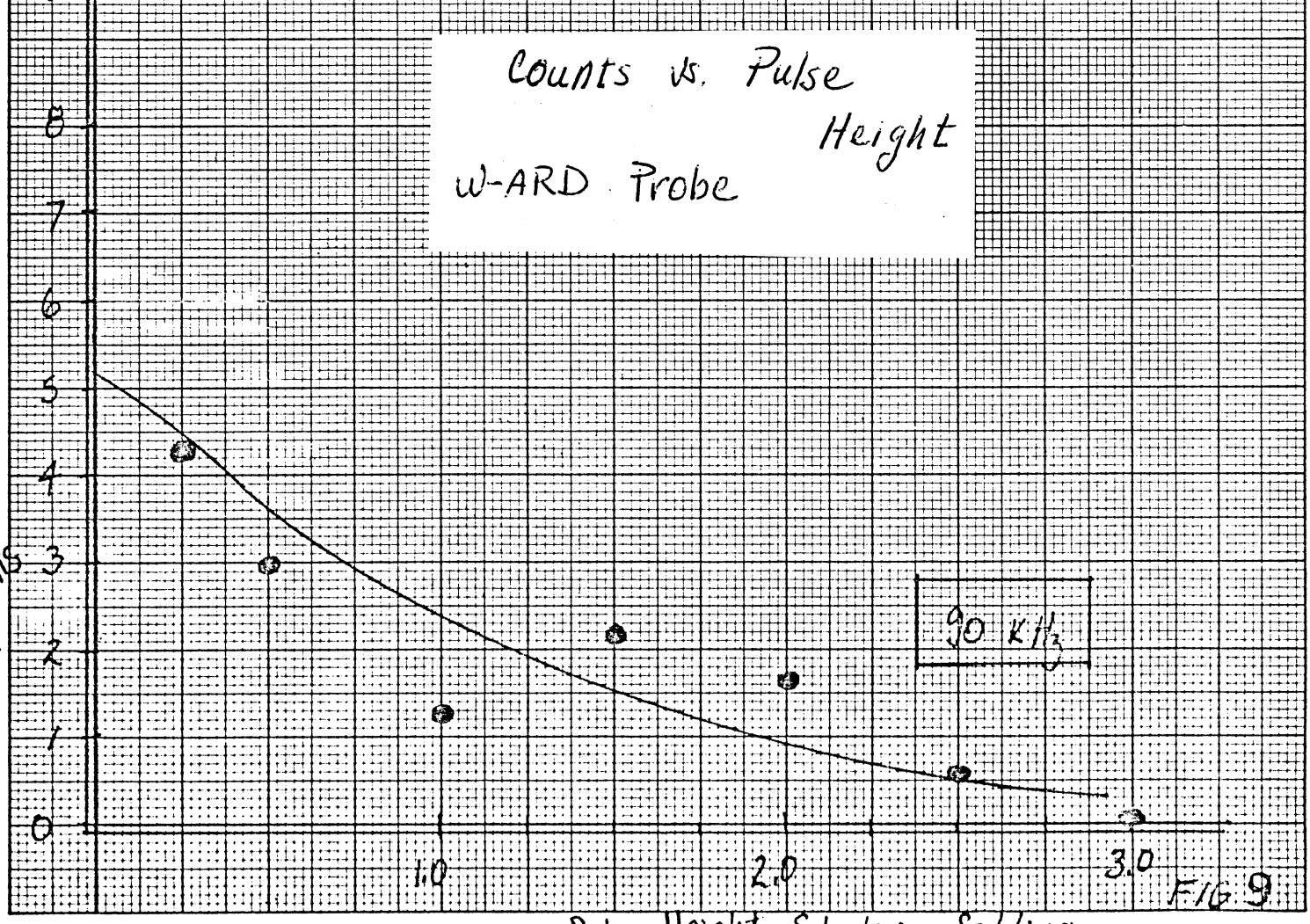

FIG 9

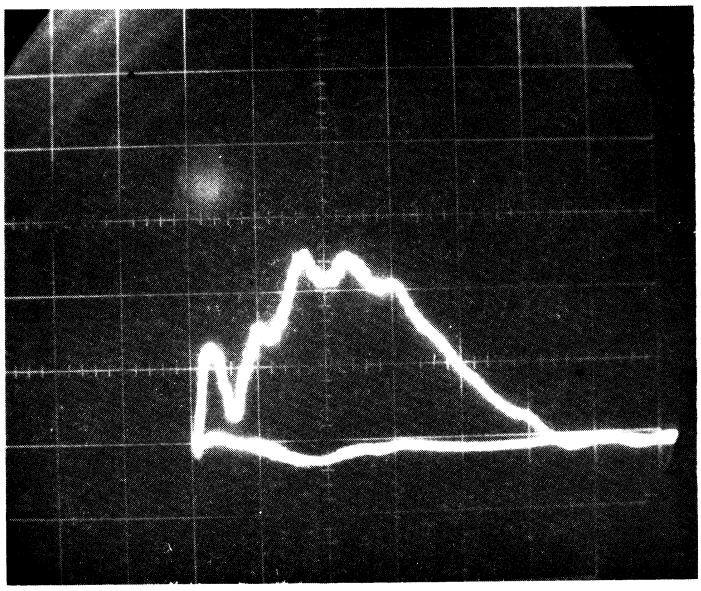

TYPICAL KISTLER OUTPUT
.2v/cm; 100μsec/cm

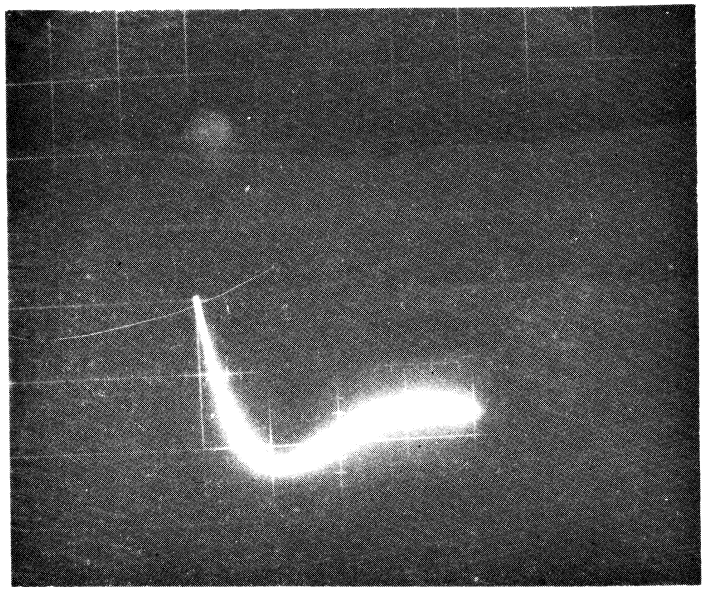

U-M HIGH-TEMP PROBE OUTPUT
1 v/cm, 100 msec/cm

FIG 10

Momentum vs. V_{max} ↑ (U-M Direct Submergence)

Monideep De
UM NUCLR ENG.
7-15-76

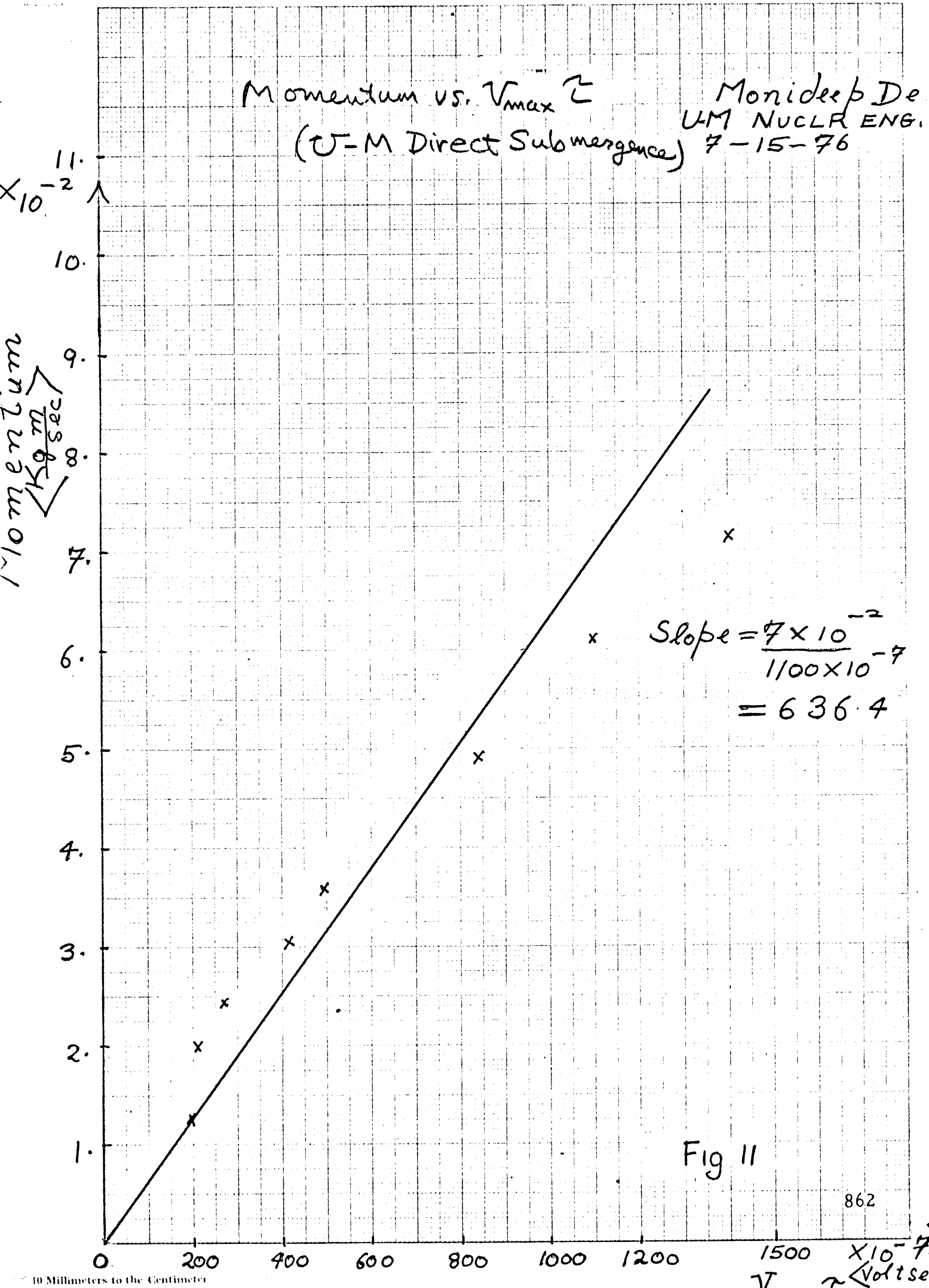

Fig 11

862

10 Millimeters to the Centimeter

Monideep De.
U-M NUCLR ENG.
7-23-76

Momentum VS V_{max}^2
(Kistler Model 603-A)

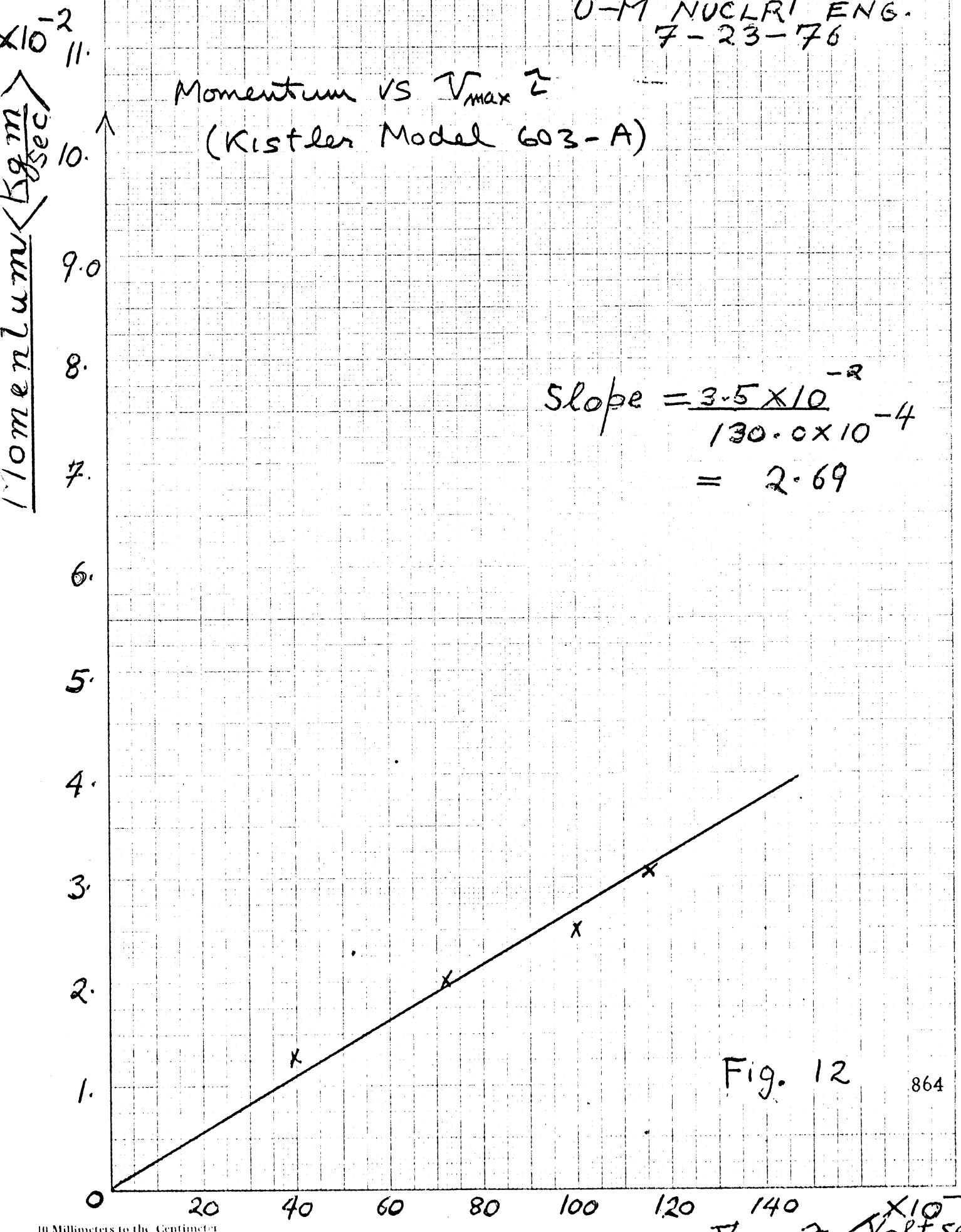

$$\text{Slope} = \frac{3.5 \times 10^{-2}}{130.0 \times 10^{-4}} = 2.69$$

Fig. 12

Table 2 Experimental Data and Calculations (Direct Submergence Probes)

a. Kistler Probe

Angle θ	Output V_{max} (volts)	τ (μ sec)	$V_{max}\,\tau \times 10^{-6}$
5	.36	550	198
7.5	.41	505	207
10.0	.52	510	265
12.5	.78	520	406
15.0	.95	520	494
20.0	1.40	600	840
25.0	1.70	650	1105
30.0	2.00	700	1400

b. U-M Direct Submergence Probe

		(m sec)	$\times 10^{-3}$
5	.36	110	39.6
7.5	.90	80	72.0
10.0	2.00	50	100.0
12.5	2.30	50	115.0

Table 3 Momentum Calculations

Θ (degrees)	$\int(1-\cos\Theta) \times 10^{-4}$	$m(2gh)^{1/2}$
5	3.98	.0126
10	14.6	.0244
15	3.2	.0360
20	58.2	.0487
25	91.2	.0609
30	126.1	.0716
35	175	.084
7.5	29.7	.0199
12.5	23.3	.0308

Probes	$\Theta = 20^{\circ}$ Applied Momentum (Kg - $\frac{m}{s}$)	Spectral Areas (volts - counts)				$\frac{\text{Applied Momentum}}{\text{Spectral Area}} \times 10^{-2}$			
		1 Hz	40 KHz	60 KHz	80 KHz	1 Hz	40 KHz	60 KHz	80 KH
Direct Submergence									
Kistler	.049	1.40				3.5			
U-M	.049	2.0				2.5			
Wave-Guide									
W-ARD	.049		6.3	6.8	4.2		.8	.72	1.17
U-M	.049		8.1	10.7	7.6		.6	.46	.64

Table 4

Overall Probe Calibration Results